Bioresource Technology 151 (2014) 36–42

Contents lists available at ScienceDirect

Bioresource Technology

journal homepage: www.elsevier.com/locate/biortech

# *In situ* synchrotron IR study relating temperature and heating rate to surface functional group changes in biomass

Kawnish Kirtania, Joanne Tanner, Kazi Bayzid Kabir, Sharmen Rajendran, Sankar Bhattacharya *

*Department of Chemical Engineering, Monash University, Clayton, VIC 3800, Australia*

## HIGHLIGHTS

- An *in situ* study by synchrotron based infrared beam on biomass pyrolysis.
- Determination of the loss of the surface functional groups with temperature.
- Comparison of the loss of functional groups as a function of heating rates.
- Retention of the surface functional groups is higher at higher heating rate.

## GRAPHICAL ABSTRACT

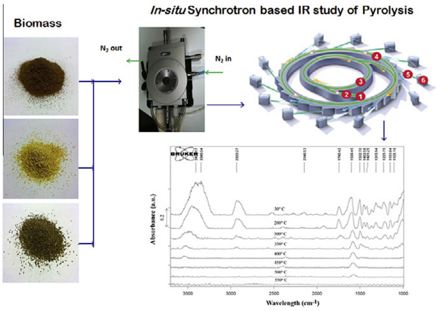

## ARTICLE INFO

*Article history:*
Received 7 August 2013
Received in revised form 7 October 2013
Accepted 10 October 2013
Available online 23 October 2013

*Keywords:*
Biomass
FTIR
Synchrotron
Pyrolysis
Heating rate

## ABSTRACT

Three types of woody biomass were investigated under pyrolysis condition to observe the change in the surface functional groups by Fourier transform infrared (FTIR) technique with increasing temperature under two different (5 and 150 °C/min) heating rates. The experiments were carried out *in situ* in the infrared microscopy beamline (IRM) of the Australian Synchrotron. The capability of the beamline made it possible to focus on single particles to obtain low noise measurements without mixing with KBr. At lower heating rate, the surface functional groups were completely removed by 550 °C. In case of higher heating rate, a delay was observed in losing the functional groups. Even at a high temperature, significant number of functional groups was retained after the higher heating rate experiments. This implies that at considerably high heating rates typical of industrial reactors, more functional groups will remain on the surface.

© 2013 Elsevier Ltd. All rights reserved.

## 1. Introduction

Biomass pyrolysis produces the biochar which can be used for several purposes such as gasification, soil enrichment and water treatment. As pyrolysis takes place in an inert atmosphere, the solid biomass decomposes throughout the process. Numerous bonds of functional groups present on the surface of the biomass produce gaseous and liquid products leaving behind solid char. During this process, the characteristics of char can change with temperature and heating rate. These operating parameters are known to have significant effects on the char properties (Di Blasi, 2009). This might also affect the kinetics of the devolatilization process depending on fuel type (Kirtania and Bhattacharya, 2012, 2013). To determine the reaction pathway of cellulose pyrolysis, Huang et al. (2013) applied density functional theory to the devolatilization process.

Literature on the loss of the surface functional groups from biomass with temperature is somewhat limited. Min et al. (2011) studied corn and wheat straw as feedstock to observe the change of the surface functional groups at low heating rate (10 °C/min) and temperatures up to 800 °C. They observed that at temperature higher than 700 °C, all the groups were lost. Rutherford et al. (2012) used nuclear magnetic resonance (NMR) and FTIR techniques to optimize the char preparation process from cellulose, lignin and pine to produce good quality biochar. They also

---

* Corresponding author. Tel.: +61 3 99059623; fax: +61 3 99055686.
*E-mail address:* sankar.bhattacharya@monash.edu (S. Bhattacharya).

0960-8524/$ - see front matter © 2013 Elsevier Ltd. All rights reserved.
http://dx.doi.org/10.1016/j.biortech.2013.10.034

observed that the initial rapid loss was caused by the aliphatic bonds and converted to aromatic carbon. This accompanied the rapid loss of oxygen rather than carbon, but some oxygen remaining after short residence time even at high temperature such as 500 °C. In another study, Zheng et al. (2013) observed the effect of torrefaction on the corncob during bio-oil production using FTIR and NMR techniques. The results showed that the oil quality can be improved by restricting crosslinking and charring during fast pyrolysis. There are few fundamental FTIR studies to identify the surface functional groups present in lignocellulosic biomass. One noteworthy work (Marcovich et al., 1996) identified all the functional groups observable on the surface of sawdust particles. However, this study did not include the loss of functional groups with temperature.

Lignocellulosic biomass can be derived from several anatomical parts of wood. Most of the biomass is extracted from the stem whereas the residues from the leaves and fruits might be also useful. An *in situ* study (Siengchum et al., 2013) examined the surface functional groups of coconut shell at different pyrolysis temperature in a diffuse reflectance infrared Fourier transform (DRIFT) cell at a heating rate of 83 °C/min. They suggested a mechanism to explain the pathway to produce oil and gas from that biomass. Another study (Sharma et al., 2004) considered lignin as their feedstock to examine the poly aromatic hydrocarbon (PAH) formation during pyrolysis. This study implied that a higher lignin content of biomass results in higher PAH formation. In an earlier study, the same authors (Sharma et al., 2002) examined the changes in the surface functional groups during tobacco pyrolysis. In the case of tobacco, the ratio of H/C was found to be decreasing after 300 °C whereas the O/C ratio was found to be constant. The variation of the behaviour indicates the diversity of biomass. It is noteworthy that all the studies discussed here were based on lab-based FTIR. Only one study on lignocellulosic biomass based on synchrotron based IR beam could be found in literature (Yu et al., 2007). This study was performed on mapping of wheat seed tissue. It demonstrated the possibilities that can be achieved by synchrotron based IR beam. However, the study did not involve the pyrolysis process.

It is well known that laboratory based IR instruments involve working with the Potassium Bromide (KBr) disks made from the mixture of KBr and crushed particles. The assumption behind these experiments is that the particles are uniformly dispersed in the disk. Also, the infrared beam is not focussed on any distinct particle and thereby, it measures the bulk surface functional groups which are the spectral average over several particles. Synchrotron based IR beam has the capability to focus on a single particle, larger than the beam size, and thereby, obtain precise information about the functional groups. So the synchrotron based IR could give the particle-wise intensity variation in the functional group content which might vary as biomass particles are not homogeneous. Moreover, it provides the opportunity to observe the visual changes during *in situ* IR measurements with temperature ramping.

The discussions above leads to this study of *in situ* assessment during pyrolysis of three types of woody biomass to observe the changes in the surface functional groups with changing temperature and heating rate by synchrotron based IR beam. The experiments were performed in the Infrared Microscopy beamline facility at Australian Synchrotron.

## 2. Methods

### 2.1. Biomass samples

Three types of biomass were used in this study – Norway spruce (*Picea abis*), wood mix from sawmill and coconut shell. The wood mix was dried and crushed to produce sawdust. The coconut shell was collected locally in Melbourne and then ground to powder form. All the samples were then dried before the experiments. The proximate and ultimate analyses of the samples are given in Table 1.

**Table 1**
Proximate and ultimate analysis (wt.%) of three biomass feedstocks.

| | Coconut shell | Spruce | Wood mix |
|---|---|---|---|
| Proximate analysis (air-dried basis) | | | |
| Moisture | 5.16 | 5.95 | 5.14 |
| Volatile matter | 69.92 | 67.89 | 65.37 |
| Fixed carbon | 24.22 | 25.66 | 24.29 |
| Ash | 0.7 | 0.5 | 5.2 |
| Ultimate analysis (dry basis) | | | |
| C | 62.45 | 44.5 | 49.50 |
| H | 6.73 | 6.55 | 6.10 |
| N | 0.43 | 0.05 | 0.15 |
| S | 0.09 | 0.04 | 0.05 |
| O[a] | 29.6 | 48.36 | 39 |
| Ash | 0.7 | 0.5 | 5.2 |

[a] By difference.

### 2.2. Selection of FTIR window

The FTIR window should be transparent enough to allow the transmission of most of the beam in its full intensity. Also in this particular case, the requirement was for high temperature resistant material as the experiment proceeds to higher temperature with time. $CaF_2$ window was used for these experiments as it can transmit almost over 90% of the intensity and it is stable up to 600 °C (ACO, 2013). A separate $CaF_2$ window was used for each sample.

### 2.3. Optical imaging

A regular microscope was attached to the instrument to visualize the condition of the particles and focus. This microscope coupled with a camera was used to capture the images of the particles periodically with changing temperature.

### 2.4. Linkam FTIR600 sample stage

The Linkam heating and cooling stage is flexible with samples and can be used either in transmission or reflection mode. Samples can be placed within a small chamber in the heating block and contains a 16 mm area for sample manipulation.

The central aperture through the sample stage is 3 mm in diameter. Samples can be either slightly larger than this and self-supporting or deposited onto the IR transmitting $CaF_2$ window which is 16 mm in diameter and 0.5–1 mm thick. In this case, the samples were powders and therefore, were dispersed on the window to measure the transmittance or absorbance.

To maintain a certain gas atmosphere, there are both gas and purge lines attached to the Linkam stage. The gas flows over the dispersed particles and removes any volatiles produced during the reaction.

### 2.5. Synchrotron light source and FTIR microscopy

The experiments were carried out using the Infrared Microspectroscopy (IRM) Beamline at Australian Synchrotron, Melbourne, Australia. The IRM beamline combines the high brilliance and high collimation of the synchrotron beam with a Bruker V80v FTIR spectrometer and a Hyperion 2000 IR microscope to reach high signal-to-noise ratios at diffraction limited spatial resolutions between 3 and 8 μm. This makes the beamline ideally suited to the analysis of microscopic samples.

Both the microscope and the spectrometer were controlled via Bruker OPUS software, version 7.2 including data acquisition, sample stage position and automated multipoint data collection. Measurements were performed using a narrow-band, high sensitivity, liquid nitrogen cooled Mercury Cadmium Telluride (MCT) detector. It was optimised for detection and data collection at a wavelength range of 3800–900 $cm^{-1}$. The aperture was set to ~10 μm × 10 μm and the resolution was 4 $cm^{-1}$. More details about the facility are available on the Australian Synchrotron website (AS, 2013).

All samples were sieved to a 20–38 μm particle size range. To make a single layer of particle on the transparent window, care was taken while dispersing. Initially $N_2$ gas was purged through the stage for 10 min. At first, the optical microscope was used to identify and select the particles of interest. To obtain more specific information, at least four particles were chosen which also served the purpose of repeating the measurement. Then an initial image of the particles was taken to identify those particles later at an elevated temperature. Measurements were recorded up to 550 °C by the infrared microscope to identify the breakage of bonds and changes in the surface functional groups. A slower heating rate of 5 °C/min was selected and the measurements were taken every 25 °C temperature increase after starting the experiment. As focus was changed with temperature, samples were refocussed at each step of temperature increase. To observe the condition of the particles visually, optical microscope was used to capture the images of the particles at all the measurement temperatures. After reaching 550 °C, an isothermal step of 10 min was programmed determining any change with time; before starting the cooling cycle. A background spectrum was collected from an area without any sample at each measurement point. A flow diagram of the experiments is shown in Fig. 1.

To link the weight loss profile with the infrared spectra, complementary pyrolysis experiments in a thermogravimetric analyser (Model STA 449 F3 Jupiter®, NETZSCH-Gerätebau GmbH, Germany) were carried out. The heating rate for the TGA experiments was selected same as the slower heating rate synchrotron IR experiments as 5 °C/min.

For higher heating rates, the surface morphology of the particles becomes different (Umeki et al., 2012; Kirtania et al., 2013) from the morphology of the particles during the devolatilization under lower heating rate. Thus, it affects the functional groups on the surface. For this, the synchrotron IR experiments at lower heating rate were repeated at a higher heating rate of 150 °C/min as well obtaining the spectra at every 25 °C temperature increase.

### 2.6. Data analysis and peak identification

Spectral data were analysed by deducting the background spectrum from the actual spectra by Bruker OPUS 7.2 software. This acted as the baseline correction and the peaks were then identified and listed based on the literature (Marcovich et al., 1996; Siengchum et al., 2013).

## 3. Results and discussion

This study presents a first *in situ* synchrotron based IR results during pyrolysis of three different biomass samples under similar conditions. The identification of the peaks was performed based on the spectra of these samples at 30 °C and listed in Table 2 for comparison. This table indicates the name of the functional groups that were available at the surface of the particles before starting the *in situ* pyrolysis and FTIR experiments.

Woody biomass consists of cellulose, hemicellulose and lignin as their building blocks. With temperature increase, these structural blocks decompose over time. Initially drying takes place up to 200 °C. After reaching 200 °C, drastic change in the functional groups takes place forming numerous long chain intermediate species. Upon increasing the temperature, these intermediate species get transformed into gas or liquid depending on the heating rate and temperature. These components break down to mostly smaller aromatic compounds and other smaller molecules. During this process, the surface functional groups of biomass disappear gradually in an orderly manner as loosely bound groups (water, some oxygen containing groups, aliphatic bonds) would disappear earlier than the strictly bound groups (some recalcitrant oxygen containing groups, aromatic bonds).

The intensity of all the functional groups was decreasing from the surface of the spruce with increasing temperature at a heating rate of 5 °C/min. A few groups that became extinct from the spectra were the absorbed water in crystalline cellulose (1660), C–H deformation with $CH_2$ bonds (1460), some skeletal C–O (1106) and syringyl ring breathing with C–O stretching from lignin (1315) at 300 °C. Subsequently, more peaks started to disappear from the spectra. With another 25 °C temperature increase, all the groups with C–H deformation were lost along with some phenolic O–H groups. At 350 °C, the carbonyl group was lost completely. After 450 °C, only three peaks were visible even though the intensity of the spectra was quite low compared to the raw samples. The toughest surface functional groups were found to be O–H stretch (3564), aromatic skeletal vibration (1569) and aromatic C–H deformation (1015) as they were still visible at a higher temperature. At about 500 °C, no further peaks were visible meaning that after 500 °C, the spruce lost all the surface functional groups at the lower heating rate. It should be noted that as the heating rate was low, the residence time in the sample stage was significantly long (around 100 min).

As the FTIR readings were taken at different stages of weight loss of the particle, a thermogravimetric plot of all the samples used is given in Fig. 2, obtained from experiments at the slow heating rate. It shows that the major weight loss takes place up to 350 °C. After this temperature, the rate of weight loss becomes very low. This agrees with the FTIR measurements that most of

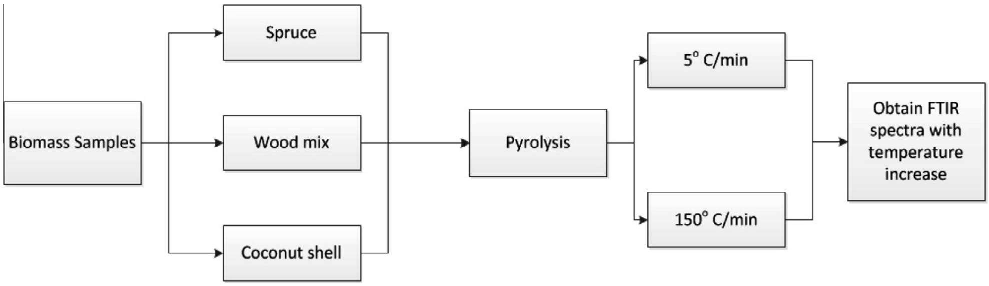

**Fig. 1.** Experimental flow diagram.

**Table 2**
Peak assignment of the IR spectra of different biomass.

| Wavelength ($cm^{-1}$) | Spruce | Wood mix | Coconut shell | Reference |
|---|---|---|---|---|
| 3388–3495 | – | O–H stretch | O–H stretch | Marcovich et al. (1996) and Siengchum et al. (2013) |
| 3339–3370 | O–H stretch | – | C–H stretch | Marcovich et al. (1996) and Siengchum et al. (2013) |
| 2903–2938 | C–H stretch | C–H stretch | C–H | Marcovich et al. (1996) and Siengchum et al. (2013) |
| 1741–1752 | C–O from carbonyl | C–O from carbonyl | C=O | Marcovich et al. (1996) and Siengchum et al. (2013) |
| 1661–1668 | Absorbed water in non-crystalline cellulose | – | C=C stretch | Marcovich et al. (1996) and Siengchum et al. (2013) |
| 1585–1606 | Ar. skeletal ring vibration | Aromatic skeletal ring vibration | Aromatic | Marcovich et al. (1996) and Siengchum et al. (2013) |
| 1503 | Same | Same | Same | |
| 1458–1465 | C–H deformation and $CH_2$ | C–H deformation and $CH_2$ | C–H deformation | Marcovich et al. (1996) and Siengchum et al. (2013) |
| 1417–1425 | C–H deformation $CH_2$ | Same | Same | |
| 1366–1372 | C–H deformation sym | C–H deformation Symmetric | C–H deformation Symmetric | Marcovich et al. (1996) and Siengchum et al. (2013) |
| 1314–1319 | Syringyl ring breathing with C–O stretching (lignin) and $CH_2$ in cellulose | Syringyl ring breathing with C–O stretching (lignin) and $CH_2$ in cellulose | Syringyl ring breathing with C–O stretching (lignin) and $CH_2$ in cellulose | Marcovich et al. (1996) and Siengchum et al. (2013) |
| 1264–1267 | Phenolic O–H | – | – | Marcovich et al. (1996) |
| 1215–1228 | Phenolic O–H deformation | Phenolic O–H deformation | C–O–C | Marcovich et al. (1996) and Siengchum et al. (2013) |
| 1164 | C–O–C stretch | C–O–C stretch | C–O–C | Marcovich et al. (1996) and Siengchum et al. (2013) |
| 1122 | – | – | Assoc. O–H, C–O–H | Siengchum et al. (2013) |
| 1104–1110 | Skeletal C–O | Skeletal vibration involving C–O stretching | – | Marcovich et al. (1996) |
| 1056–1059 | Skeletal C–O | – | – | Marcovich et al. (1996) |
| 1032 | Ar. C–H deformation | Ar. C–H deformation | – | Marcovich et al. (1996) |

the functional groups were lost around 350 °C at slower heating rate.

Lignin is known to be the toughest building block of biomass for volatile release. It starts to decompose earlier than cellulose and hemi-cellulose but the decomposition progresses later than the other two. It can be noted that most of the remaining functional groups at a higher temperature are from lignin (Rutherford et al., 2012). Amongst the kinetics of cellulose, hemi-cellulose and lignin decomposition, the activation energy of lignin is less than the activation energy of the cellulose and hemi-cellulose. But the lignin survives longer than the other two at a higher temperature such as 723 °C (Orfao et al., 1999; Rao and Sharma, 1998). Moreover, due to the aromaticity of lignin char, it is less reactive compared to the char produced from cellulose and hemicellulose (Sharma et al., 2004). So the aromatic skeletal vibration was remaining in lignin for longer time at the highest temperature under this study.

To assess the effect of heating rate, higher heating rate of 150 °C/min, the highest heating rate permissible by the instrument was used. This took only 3.5 min to reach over 500 °C. With additional time taken to obtain the spectra at different temperatures, the cumulative time was slightly higher than 3.5 min. In comparison to the lower heating rate experiments, some functional groups retained their existence at higher temperature. Up to 350 °C, only two obvious functional groups were completely lost–absorbed water in crystals and syringyl ring with C–O stretching. When the temperature was ramped up to 400 °C, two more functional groups were lost. At 500 °C, five peaks were still visible (O–H stretch, C–O, Ar. Skeletal vibration, some skeletal C–O and Ar. C–H deformation). After 550 °C, only one functional group was left (Aromatic skeletal vibration). This provides an indication about the effect of heating rate. Even though, the heating rate will be significantly higher(Bell et al., 2011) in other reactors, such as in wire mesh reactor (up to 1000 °C/s) and in the industrial cases (up to 10,000 °C/s), these experiments give an indication of the consequence of the higher heating rate on functional groups. This loss of the functional groups will be delayed in case of higher heating rate.

The functional groups were not significantly different in the spectra of the other two samples as both of these were derived from wood. The wood mix showed slightly different behaviour than the pure spruce sawdust. During the slow heating rate experiment, only one group (C–O from carbonyl) was lost up to 350 °C. After 400 °C, six functional groups were lost and at 450 °C, the O–H stretch was also lost. Only aromatic skeletal vibration (C–C) was observed to be remaining at 500 °C. As before, all the groups were lost at 550 °C. A closer observation of both the spectra revealed that the intensity of the spectral peaks were not the same even though they were obtained from the same sample. This confirmed the non-homogeneity of the wood mix. As a different particle was chosen for the higher heating rate experiments, the spectral peaks were the same but the intensity changed. However, this intensity change behaviour was not significantly different from the pure spruce sawdust under study. It implies that the non-homogeneity of the wood mix was comparable with the spruce as far as the infrared spectral intensity of the surface functional groups under concern. In case of the faster heating rate, only the absorbed water and syringyl ring with C–O stretching were lost at 400 °C. Some traces of the oxygen containing functional groups such as C–O, O–H were found to be retained up to 550 °C. This is important in case of subsequent gasification of the char. The oxygen containing groups may affect the reactivity by taking part in the reaction. The points of measurement on the rate of weight loss curve are identified in Fig. 2b. This graph also agrees with the FTIR data in that the weight loss rate became significantly higher after 300 °C, and then came back to zero after 360 °C when almost all the groups containing oxygen and hydrogen became undetectable.

The functional groups of coconut shell were lost faster than the other two samples. By 450 °C, all the functional groups were lost from the surface at lower heating rate. The peak heights decreased after 300 °C drastically. Even the aromatic skeletal vibration of the

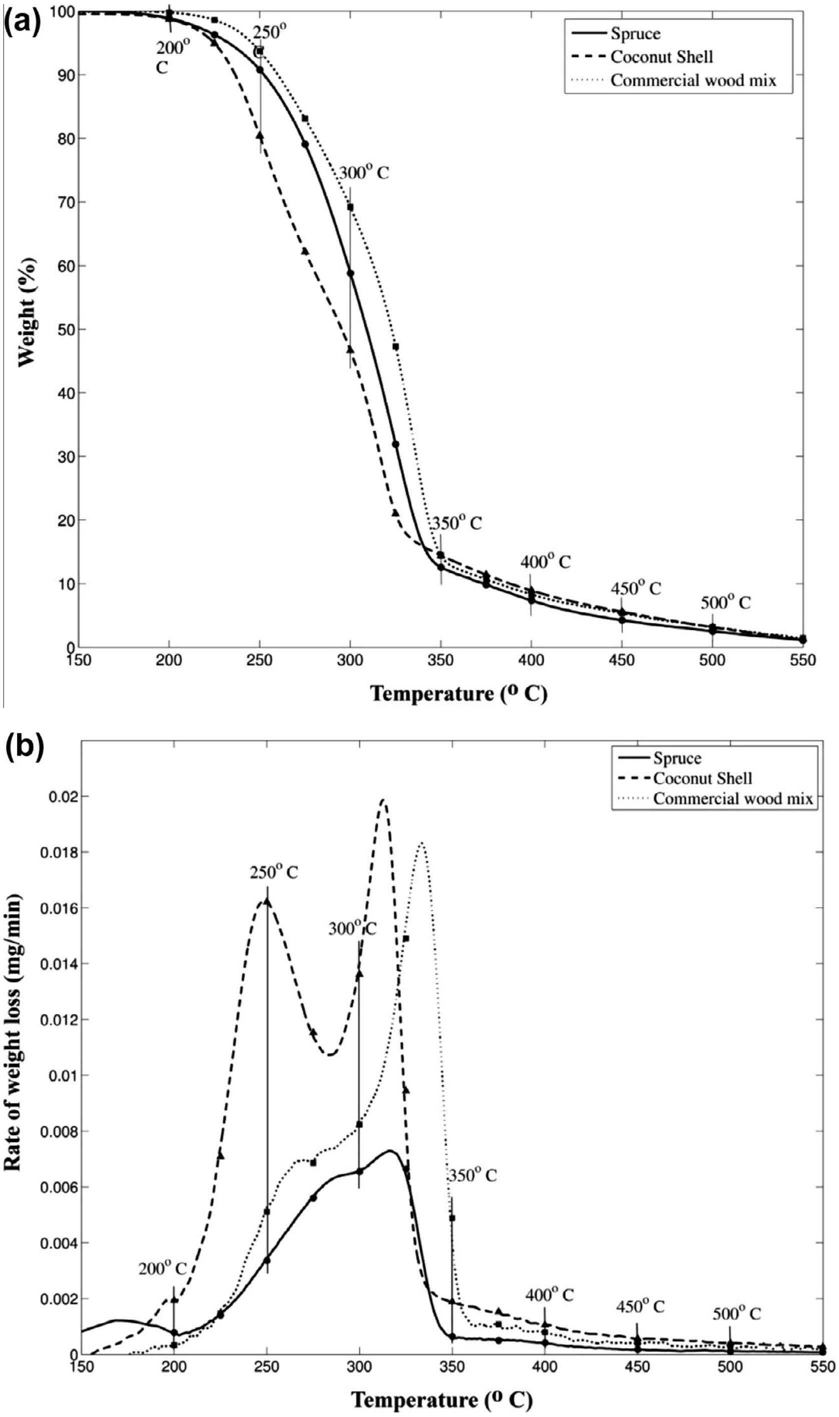

**Fig. 2.** FTIR measurement points on thermogravimetric curve. (a) Weight loss characteristics, (b) rate of weight loss.

carbon bonds was not visible at 450 °C. At higher heating rate, some groups were retained up to 550 °C. The groups remaining after 550 °C were – aromatic skeletal vibration and C–H deformation. Fig. 2b shows the rate of weight loss for coconut shell at lower heating rate. As evident from the figure, coconut shell lost its volatile components in two stages. The first stage took place between 200 and 275 °C and the second stage was in between 275 and 330 °C. The second stage showed highest rate of volatile loss. Even though it took two stages of weight loss, it finished earlier than both the wood mix and spruce. Also because of these two steps, the peaks in the FTIR readings were observed to lose their intensity faster after 200 °C than the other biomass. Interestingly, the coconut shell retained two functional groups (aromatic skeletal vibration and C–H deformation from $CH_2$) at higher heating rate but it lost all other groups after 400 °C.

Table 3 shows the summary of the effect of heating rate on different surface functional groups at different temperature in the three biomass samples. As the visual changes of the particles were recorded by the CCD camera, the shrinkage of the particles for all three samples was evident. The cluster of particles which were opaque initially became clear and isolated at 550 °C after pyrolysis. Some groups of particles were converted to a distorted single particle. Though shrinkage is not considered during particle modelling of pyrolysis (Bellais et al., 2003), the observation implies that the

**Table 3**
List of functional groups remaining at higher temperatures under different heating rates.

| Functional groups | Band | 300 °C |  | 350 °C |  | 400 °C |  | 450 °C |  | 500 °C |  | 550 °C |  |
|---|---|---|---|---|---|---|---|---|---|---|---|---|---|
|  |  | Slow | Fast | Slow | Fast | Slow | Fast | Slow | Fast | Slow | Fast | Slow | Fast |
| O–H stretch | 3388–3495 | C, W | C, W | C, W | C, W | C, W | C, W | – | W | – | W | – | – |
| O–H stretch | 3339–3370 | C,S | C,S | S | – | S | S | S | S | – | S | – | – |
| C–H stretch | 2903–2938 | C, W, S | C, W, S | C, W, S | C, W | S | W ,S | W | W, S | – | W | – | – |
| C–O from carbonyl | 1741–1752 | C, W, S | C, W, S | C | C | C | C,S | – | S | – | S | – | – |
| Absorbed water in non-crystalline cellulose | 1661–1668 | – | – | – | – | – | – | – |  | – | – | – | – |
| Ar. skeletal vibration | 1585–1606 | C, W, S | C, W, S | C, W, S | C, W, S | C, W, S | C, W, S | W, S | C, W, S | W | C, W, S | – | C, W, S |
| Same | 1503 | C, W, S | C, W, S | C, W | C, W, S | – | S | – |  | – | – | – | – |
| C–H deformation and $CH_2$ | 1458–1465 | C, W | C, W, S | W | W, S | – | W ,S | – | W | – | W | – | W |
| C–H deformation $CH_2$ | 1417–1425 | C, W, S | C, W, S | W, S | C, W, S | S | C, W, S | – | C | – | C | – | C |
| C–H deformation sym | 1366–1372 | C | C, W, S | – | W |  |  |  |  | – | – | – | – |
| Syringyl ring breathing with C–O stretching (lignin) and $CH_2$ in cellulose | 1314–1319 | C | C, W | – | – | – | – | – | – | – | – | – | – |
| Phenolic O–H | 1264–1267 | S | S | – | S | – | S | – | S | – | – | – | – |
| Phenolic O–H deformation | 1215–1228 | C, W, S | C, W, S | W, S | W, S | – | W ,S | – | W, S | – | – | – | – |
| C–O–C stretch | 1164 | C, W, S | C, W, S | W | W, S | – | W ,S | – | W | – | W | – | W |
| Assoc. O–H, C–O–H | 1122 | C | C | – | – | – | – | – |  | – | – | – | – |
| Skeletal C–O | 1104–1110 | C, W | C, W, S | W, S | C, W | S | W | – |  | – | – | – | – |
| Skeletal C–O | 1056–1059 | S | S | W, S |  | S | W | – | W, S | – | S | – | – |
| Ar. C–H deformation | 1032 | W, S | W, S | W, S | W, S | W, S | W ,S | S | W, S | – | W, S | – | W |

C = coconut shell, W = wood mix, S = spruce.

shrinkage might be necessary to be taken into account for robust pyrolysis modelling.

## 4. Conclusion

The disappearance of the surface functional groups with temperature was studied using *in situ* synchrotron IR measurements during pyrolysis of three woody biomass up to 550 °C at different heating rates. The results confirmed the heterogeneity of biomass particles. The results from the higher heating rate experiments showed a lag in the release of surface functional groups leading to more functional groups retained after pyrolysis. This effect should be considered for optimizing the pyrolysis process of biomass, if subsequent use of the biochar through thermochemical processing is intended. The experiments demonstrate the usefulness of synchrotron IR spectroscopy for pyrolysis investigation.

## Acknowledgements

Infrared Microscopy Beamline Facilities at Australian Synchrotron (Experiment ID-M6001) have been used to carry out the experiments. The authors thank Dr. Mark Tobin and Dr. Lauren Hyde of Australian Synchrotron for their help during running the experiments and assistance for data analyses.

## Appendix A. Supplementary data

Supplementary data associated with this article can be found, in the online version, at http://dx.doi.org/10.1016/j.biortech.2013.10.034.

## References

ACO – Alkor Crystal Optics, 2013, Available online at <http://www.alkor.net/CaF2.html> (accessed 27.07.13).

Australian Synchrotron, 2013, Available online at <http://www.synchrotron.org.au/index.php/aussyncbeamlines/infrared-micro/technical-information2> (accessed 27.07.13).

Bellais, M., Davidsson, K.O., Liliedahl, T., Sjostrom, K., Pettersson, J.B.C., 2003. Pyrolysis of large wood particles: a study of shrinkage importance in simulations. Fuel 82, 1541–1548.

Blasi, C.D., 2009. Combustion and gasification rates of lignocellulosic chars. Prog. Energy Combust. Sci. 35, 121–140.

Bell, D.A., Towler, B.F., Fan, M., 2011. Coal Gasification and its Applications, first ed. Elsevier Inc., Oxford, UK.

Huang, X., Cheng, D., Chen, F., Zhan, X., 2013. Reaction pathways of β-D-glucopyranose pyrolysis to syngas in hydrogen plasma: a density functional theory study. Bioresour. Technol. 143, 447–454.

Kirtania, K., Bhattacharya, S., 2012. Application of distributed activation energy model to the kinetic study of pyrolysis of fresh water algae *Chlorococcum humicola*. Bioresour. Technol. 107, 476–481.

Kirtania, K., Bhattacharya, S., 2013. Pyrolysis kinetics and reactivity of algae-coal blends. Biomass Bioenergy 55, 291–298.

Kirtania, K., Joshua, J., Kassim, M. A., Bhattacharya, S., 2013. Comparison of $CO_2$ and steam gasification reactivity of algal and woody biomass. Fuel Process. Technol. (in press), http://dx.doi.org/10.1016/j.fuproc.2013.02.006.

Marcovich, N.E., Reboredo, M.M., Aranguren, M.I., 1996. FTIR spectroscopy applied to woodflour. Compos. Interface 4 (3), 119–132.

Min, F., Zhang, M., Zhang, Y., Cao, Y., Pan, W.P., 2011. An experimental investigation into the gasification reactivity and structure of agricultural waste chars. J. Anal. Appl. Pyrolysis 92, 250–257.

Orfao, J.J.M., Antunes, F.J.A., Figueiredo, J.L., 1999. Pyrolysis kinetics of lignocellulosic materials-three independent reactions model. Fuel 78, 349–358.

Rao, T.R., Sharma, A., 1998. Pyrolysis rates of biomass materials. Energy 23, 973–978.

Rutherford, D.W., Wershaw, R.L., Rostad, C.E., Kelly, C.N., 2012. Effect of formation conditions on biochars: compositional and structural properties of cellulose, lignin, and pine biochars. Biomass Bioenergy 46, 693–701.

Sharma, R.K., Wooten, J.B., Baliga, V.L., Martoglio-Smith, P.A., Hajaligol, M.R., 2002. Characterization of char from the pyrolysis of tobacco. J. Agric. Food Chem. 50, 771–783.

Sharma, R.K., Wooten, J.B., Baliga, V.L., Lin, X., Geoffrey, C.W., Hajaligol, M.R., 2004. Characterization of chars from pyrolysis of lignin. Fuel 83, 1469–1482.

Siengchum, T., Isenberg, M., Chuang, S.S.C., 2013. Fast pyrolysis of coconut biomass – an FTIR study. Fuel 105, 559–565.

Umeki, K., Kirtania, K., Chen, L., Bhattacharya, S., 2012. Fuel particle conversion of pulverized biomass during pyrolysis in an entrained flow reactor. Ind. Eng. Chem. Res. 51 (43), 13973–13979.

Yu, P., Block, H., Niu, Z., Doiron, K., 2007. Rapid characterization of molecular chemistry, nutrient make-up and microlocation of internal seed tissue. J. Synchrotron Radiat. 14, 382–390.

Zheng, A., Zhao, Z., Chang, A., Huang, Z., Wang, X., He, F., Li, H., 2013. Effect of torrefaction on structure and fast pyrolysis behaviour of corncobs. Bioresour. Technol. 128, 370–377.